SANDIA REPORT
SAND2009-7981
Unlimited Release
Printed January 2010

Imaging Doped Silicon Test Structures Using Low Energy Electron Microscopy

M. L. Anderson, C. Y. Nakakura, G. L. Kellogg

Prepared by
Sandia National Laboratories
Albuquerque, New Mexico 87185

Sandia is a multiprogram laboratory operated by Sandia Corporation,
a Lockheed Martin Company, for the United States Department of Energy's
National Nuclear Security Administration under Contract DE-AC04-94AL85000.

Approved for public release; further dissemination unlimited.

Sandia National Laboratories

Issued by Sandia National Laboratories, operated for the United States Department of Energy by Sandia Corporation.

NOTICE: This report was prepared as an account of work sponsored by an agency of the United States Government. Neither the United States Government, nor any agency thereof, nor any of their employees, nor any of their contractors, subcontractors, or their employees, make any warranty, express or implied, or assume any legal liability or responsibility for the accuracy, completeness, or usefulness of any information, apparatus, product, or process disclosed, or represent that its use would not infringe privately owned rights. Reference herein to any specific commercial product, process, or service by trade name, trademark, manufacturer, or otherwise, does not necessarily constitute or imply its endorsement, recommendation, or favoring by the United States Government, any agency thereof, or any of their contractors or subcontractors. The views and opinions expressed herein do not necessarily state or reflect those of the United States Government, any agency thereof, or any of their contractors.

Printed in the United States of America. This report has been reproduced directly from the best available copy.

Available to DOE and DOE contractors from
U.S. Department of Energy
Office of Scientific and Technical Information
P.O. Box 62
Oak Ridge, TN 37831

Telephone: (865) 576-8401
Facsimile: (865) 576-5728
E-Mail: reports@adonis.osti.gov
Online ordering: http://www.osti.gov/bridge

Available to the public from
U.S. Department of Commerce
National Technical Information Service
5285 Port Royal Rd.
Springfield, VA 22161

Telephone: (800) 553-6847
Facsimile: (703) 605-6900
E-Mail: orders@ntis.fedworld.gov
Online order: http://www.ntis.gov/help/ordermethods.asp?loc=7-4-0#online

SAND2009-7981
Unlimited Release
Printed January 2010

Imaging Doped Silicon Test Structures Using Low Energy Electron Microscopy

Meredith L. Anderson
Craig Y. Nakakura
Gary L. Kellogg

Sandia National Laboratories
P.O. Box 5800
Albuquerque, New Mexico 87185

Abstract

This document is the final SAND Report for the LDRD Project 105877 – "Novel Diagnostic for Advanced Measurements of Semiconductor Devices Exposed to Adverse Environments" – funded through the Nanoscience to Microsystems investment area.

CONTENTS

1. Introduction 5
2. Imaging Oxide-Covered Doped Si Structures Using LEEM 6
Distribution 13

1. INTRODUCTION

Along with the continuous decrease in the feature size of semiconductor device structures comes a growing need for inspection tools with high spatial resolution and high sample throughput. Ideally, such tools should be able to characterize both the surface morphology and local conductivity associated with the structures. The imaging capabilities and wide availability of scanning electron microscopes (SEMs) make them an obvious choice for imaging device structures. Dopant contrast from *pn* junctions using secondary electrons in the SEM was first reported in 1967 [1] and more recently starting in the mid-1990s [2-6]. However, the serial acquisition process associated with scanning techniques places limits on the sample throughput.

Significantly improved throughput is possible with the use of a parallel imaging scheme such as that found in photoelectron emission microscopy (PEEM) and low energy electron microscopy (LEEM). The application of PEEM and LEEM to device structures relies on contrast mechanisms that distinguish differences in dopant type and concentration. Interestingly, one of the first applications of PEEM was a study of the doping of semiconductors, which showed that the PEEM contrast was very sensitive to the doping level and that dopant concentrations as low as 10^{16} cm^{-3} could be detected [7]. More recent PEEM investigations of Schottky contacts were reported in the late 1990s by Giesen et al. [8], followed by a series of papers in the early 2000s addressing doping contrast in PEEM by Ballarotto and co-workers [9-13] and Frank and co-workers [14].

In contrast to PEEM, comparatively little has been done to identify contrast mechanisms and assess the capabilities of LEEM for imaging semiconductor device strictures. The one exception is the work of Mankos et al. [15], who evaluated the impact of high-throughput requirements on the LEEM designs and demonstrated new applications of imaging modes with a tilted electron beam. To assess its potential as a semiconductor device imaging tool and to identify contrast mechanisms, we used LEEM to investigate doped Si test structures. In section 2, Imaging Oxide-Covered Doped Si Structures Using LEEM [16], we show that the LEEM technique is able to provide reasonably high contrast images across lateral *pn* junctions. The observed contrast is attributed to a work function difference ($\Delta\phi$) between the *p*- and *n*-type regions. However, because the doped regions were buried under a thermal oxide (~3.5 nm thick), e-beam charging during imaging prevented quantitative measurements of $\Delta\phi$. As part of this project, we also investigated a series of similar test structures in which the thermal oxide was removed by a chemical etch. With the oxide removed, we obtained intensity-versus-voltage (I-V) curves through the transition from mirror to LEEM mode and determined the relative positions of the vacuum cutoffs for the differently doped regions. Although the details are not discussed in this report, the relative position in voltage of the vacuum cutoffs are a direct measure of the work function difference ($\Delta\phi$) between the *p*- and *n*-doped regions.

2. IMAGING OXIDE-COVERED DOPED SI STRUCTURES USING LEEM

In this section, low energy electron microscopy (LEEM) operated at incident electron energies just above the "mirror" mode is used to image Si-based test devices. Significant *p*- vs. *n*- doping contrast is observed, even when the structures are covered with a ~3.5 nm thermal oxide. The contrast arises from a difference in surface potential between the two regions and is related to both *p*-*n* work function differences and electron-beam-induced charging of the oxide. The results show that the LEEM is capable of characterizing *pn* junctions without complicated sample preparation and that it is a promising technique for rapid, non-destructive imaging of microelectronic devices.

The experiments detailed in this section were performed using a commercial LEEM (Elmitec, LEEM III) [17]. In this type of microscope (see Figure 1), high-energy electrons (20 kV) from an electron gun (a LaB_6 source in our system) are focused on the back focal plane of an objective lens producing a parallel beam at the sample surface. Low electron energies at the sample are achieved by biasing it at a negative potential near to that of the source. The difference between the source and sample potential is called the start voltage, V_s. Depending on the value of V_s (-2 to +3 V in this study), electrons are either reflected (mirror electron microscopy, MEM) or scattered (LEEM) from the surface. The image formed by the objective lens using these electrons are re-accelerated to 20 kV, transferred by a magnetic prism, magnified by a series of lenses and projected on to a viewing screen.

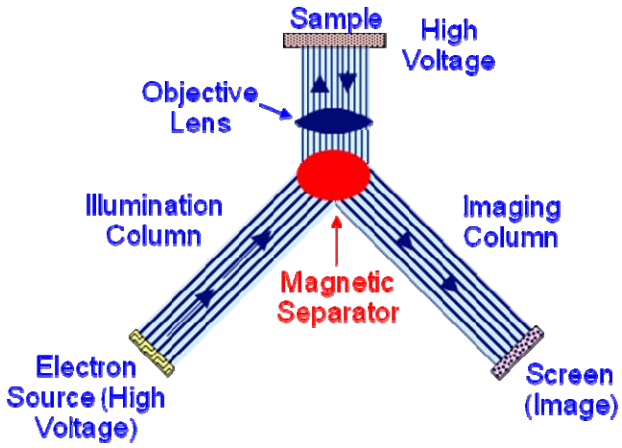

Figure 1. Schematic of a low-energy electron microscope.

Figure 2 shows a plot of how the reflected or scattered electron intensity varies as a function of V_s at low electron energies. When the sample potential is more negative than the gun potential (MEM), electrons are reflected before hitting the surface and the intensity is at its maximum. When the start voltage exceeds an onset potential (V_{onset}, also referred to as the vacuum cutoff), electrons flow and the reflected electron intensity goes down. The onset occurs when the vacuum energy levels of the gun and sample align, so the onset voltage is given by the difference in work function between the sample and electron gun. As the start voltage is further increased, the intensity becomes higher due to the increase in backscattered electrons as a function of electron energy. We refer to these plots of intensity as a function of start voltage as "I-V curves." The range of start voltages where these changes in intensity occur is typically from -3 V to 0 V. When there are two regions on a surface with different work functions, the onset voltage occurs at different voltages. As shown below, by choosing the appropriate start voltage for imaging, there can be significant contrast based on the work function difference between the two regions.

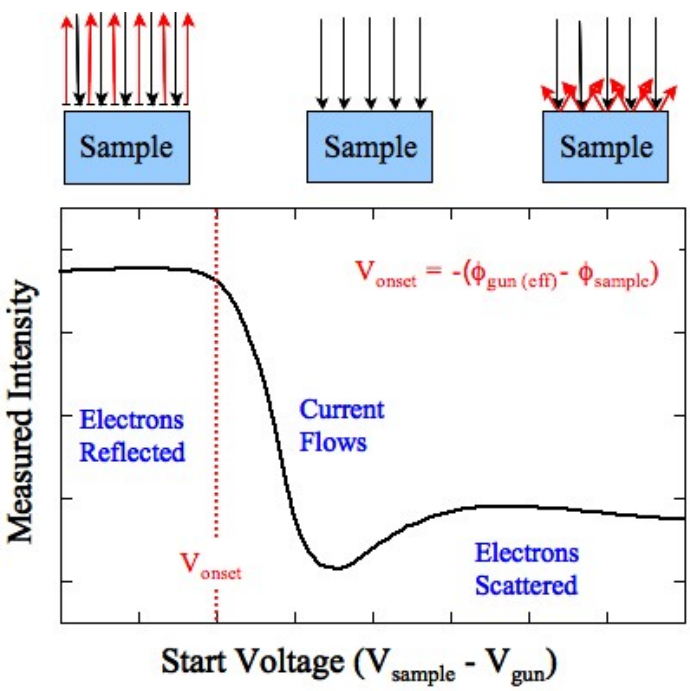

Figure 2. An I-V curve showing the general behavior of the measured intensity as a function of increasing start voltage when changing from the MEM to LEEM imaging modes.

The diode test structures used in this study were fabricated at Sandia National Laboratories MESA facility. Arsenic (As) and/or boron (B) were implanted into Si(100) *p*-type substrates to construct n^+/p junctions. Figure 3 shows cross-sectional (a) and top-down (b) schematics of the structures. A thermal oxide of ~ 3.5 nm thickness is indicated in (a). The regions of *n* vs. *p* doping are shown in (b). The doping concentration of the *n*-type region (blue) is ~10^{17} cm^{-3}. A series of *n*-type lines ranging in width from 0.25 μm to 1.1 μm extend into the *p*-type region (red) with a concentration of ~10^{19} cm^{-3}. The black circles on (b) indicate two locations where

LEEM images (shown below) were acquired. Sample preparation consisted of sonicating the test structures in isopropyl alcohol.

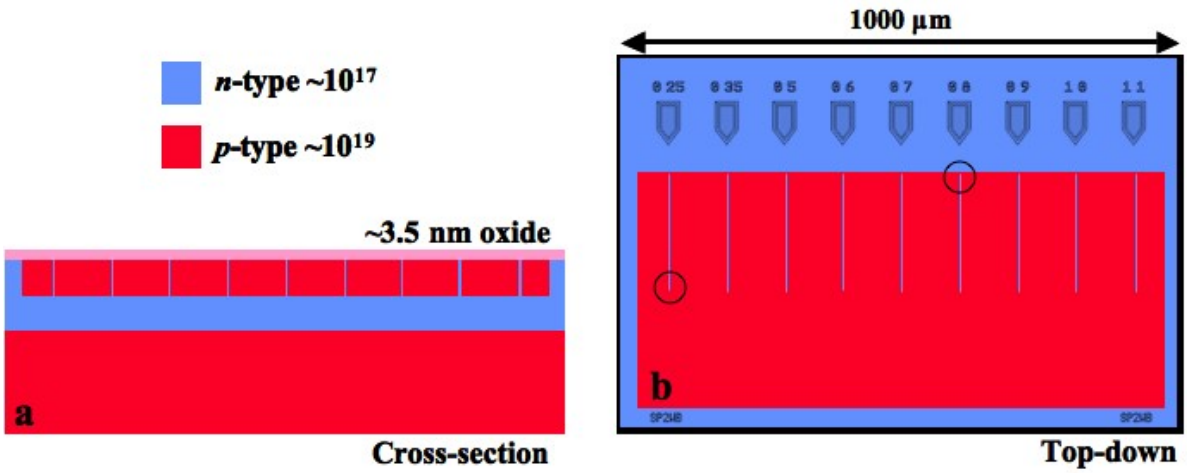

Figure 3. (a) Cross-sectional and (b) top-down schematics of test structures imaged with LEEM.

Figure 4 shows 20 µm field-of-view LEEM images of the *n*-type lines (widths of 0.25 µm, 0.5 µm, and 0.8 µm). The position of the acquired image in Figure 3(a) is indicated by the bottom left circle in Figure 3(b). The *p*-type region appears bright and the *n*-type lines appear dark at a start voltage of 1.0 V. The widths of the lines determined from the images are found to vary with imaging conditions, but are typically within 20% of the doping line widths. Given the presence of the thermal oxide on the surface and the minimal sample preparation procedures, the observation of *p*-*n* contrast in the LEEM was quite unexpected.

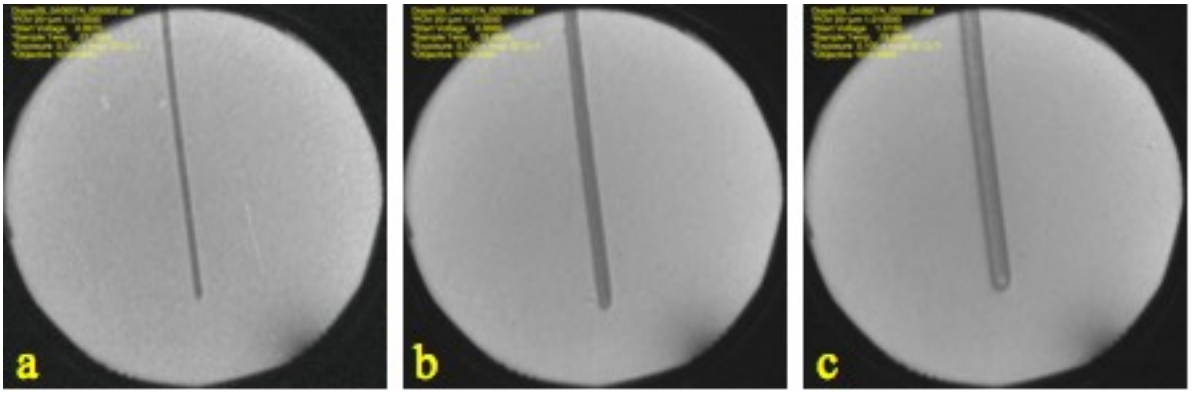

Figure 4. LEEM images of *n*-type lines a) 0.25 µm, b) 0.5 µm, and c) 0.8 µm, with *p*-type background, 20 µm field of view.

Figure 5 shows how the *p*-*n* contrast varies as a function of start voltage. Three images of the 0.5 µm line are shown at start voltages of -2.00 V, -0.15 V, and 0.70 V. It is clear from the figure that the contrast reverses when increasing the start voltage from -0.15 V to 0.70 V. This reversal is understood in terms of the I-V curves from the *n*- and *p*-type regions shown in Figure 6. With V_s = -2.0 V (Figure 4a) both the *n*- and *p*-type regions are bright. This corresponds to the MEM mode where electrons are reflected and the intensity is at its maximum for both the *n*-

and *p*-type regions. When V_s = -0.15 V (Figure 5b), the *n*-type region is dark and *p*-type region is bright. This voltage is above the onset voltage for current flow for the *n*-type region, but below that for the *p*-type region. Electrons are reflected from the *p*-type region (bright) but there is current flowing in the *n*-type region (dark). In (c), with V_s = 0.7 V, the intensity from the *n*-type region is higher because the number of backscattered electrons has increased. The intensity of the *p*-type region is lower because the onset voltage this region has been exceeded. The fact that V_{onset} occurs at a more negative voltage for the *n*-type area in Figure 6 is expected since the work function of *n*-type Si is smaller than for *p*-type. However, the separation between the I-V curves (1.5 V) is significantly larger than the work function difference between *n*- and *p*-type Si (0.7 eV). An additional effect is needed to account for the increased separation between the curves.

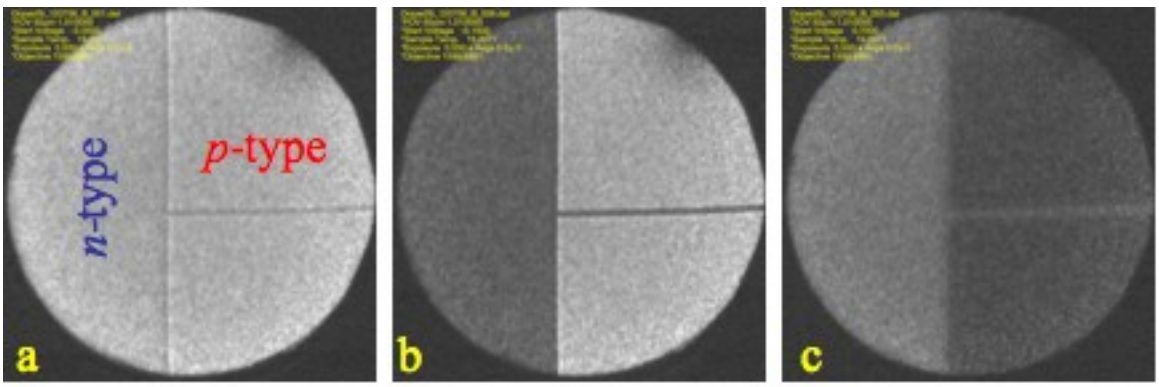

Figure 5. LEEM images of 0.5 μm *n*-type line at start voltages of a) -2.0 V, b) -0.15 V, and c) 0.7 V, 50 μm field of view.

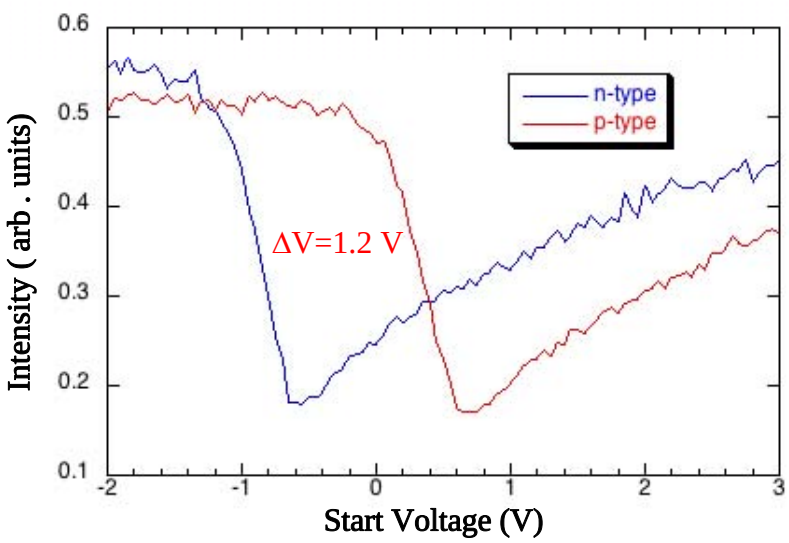

Figure 6. I-V curves for *n*- and *p*-type Si regions of test structures.

The additional effect impacting the onset voltage of the I-V curves in our experiments is electron-beam-induced charging of the thermal oxide. Clear evidence for charging is seen in Figure 7. The images are individual frames taken from a video sequence during which the sample is translated under the beam. The start voltage in all three images is 0.0 V. Image (a) is recorded after allowing the intensity to stabilize for several minutes. The sample is translated in

a vertical direction to a new region just before recording image (b). The curved line separating the light and dark contrast in the *p*-type region is the edge of the beam spot. The freshly exposed *p*-type region is momentarily dark and then proceeds to get bright as a function of time. The increase in intensity is caused by a time-dependent change in surface potential. As the oxide becomes more negatively charged, the imaging mode changes from LEEM back to MEM. Eventually, the new region (c) is charged to the same potential as the initial image (a). Two points worth noting are that (1) the charged region is highly localized, as evidenced by the sharp line dividing the charged and uncharged region in (b), and (2) the charge persists for hours to days. For example, samples left overnight are still charged when imaged the next day. However, we find the regions can be "discharged" by increasing the electron energy to higher positive values (tens of volts). Here, the backscattered current exceeds the incident current and the oxide charges positively. Figure 7 also shows that the oxide above the *p*-type region has a more pronounced sensitivity to electron beam charging than that above the *n*-type region. This sensitivity, however, depends on the start voltage. When the start voltage is held at 0.0 V, as in Figure 7, the *p*-type region shows the strong time-dependent behavior. At more negative values of V_s, the intensity from the *n*-type region changes more strongly with time.

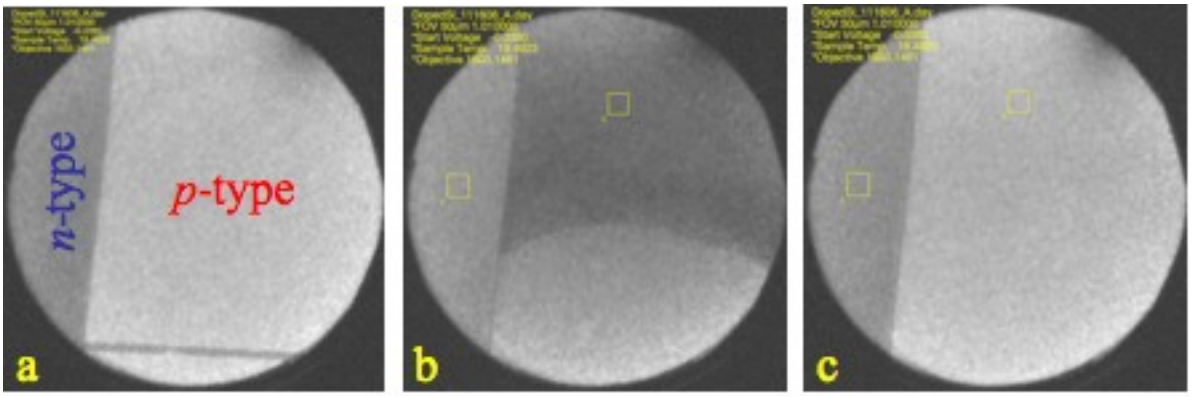

Figure 7. LEEM images showing the effect of oxide charging, start voltage = 0 V, 50 μm field of view.

The above results show that charging of the oxide by the imaging electron beam affects the surface potential that, in turn, determines the ratio of scattered to reflected electrons. This complicates the interpretation of I-V curves such as the ones in Figure 6. The difference in onset voltage is not simply the difference in work function between the two regions, but includes the difference in surface potential due to charging. This is important because the charging can depend on factors other than the *n* vs. *p* doping difference. For example, from atomic force microscope (AFM) images, we know that the thickness of the oxide above the two regions is not the same. The doping concentrations are also markedly different. So, is the contrast due to differences in *n* vs. *p* doping, difference in oxide thickness, or differences in doping concentrations? The results show that the onset voltage and thus the contrast mechanism depends on all three.

In summary, we have shown that LEEM can be used to image doped Si test structures buried under ~3.5 nm thermal oxides. The reflected/scattered electron intensity from the *n*- and *p*-type regions first decreases rapidly and then increases as a function of increasing start voltage (the sample bias relative to the electron gun bias). The start voltage at which the intensity begins to

decrease (the change from MEM to LEEM imaging modes) is shifted in voltage for regions above the two types of doping. Thus, strong contrast can be achieved by “tuning” the start voltage. We also measure time-dependent oxide charging effects that are a function of both the start voltage and buried dopant type.

REFERENCES

[1] T.H.P. Chang, W.C. Nixon, Solid-State Electronics **10** (1967) 701-&.

[2] D.D. Perovic, M.R. Castell, A. Howie, C. Lavoie, T. Tiedje, J.S.W. Cole, Ultramicroscopy **58** (1995) 104-113.

[3] A. Howie, J. Microsc. **180** (1995) 192-203.

[4] D. Venables, D.M. Maher, Journal of Vacuum Science & Technology B **14** (1996) 421-425.

[5] D. Venables, H. Jain, D.C. Collins, Journal of Vacuum Science & Technology B **16** (1998) 362-366.

[6] P. Kazemian, S.A.M. Mentink, C. Rodenburg, C.J. Humphreys, Journal of Applied Physics **100** (2006).

[7] W. Driesel, H. Bethge, Akad. Wissensch. DDR, Rossendorf, 1985, 595.

[8] M. Giesen, R.J. Phaneuf, E.D. Williams, T.L. Einstein, Surface Science **396** (1998) 411-421.

[9] V.W. Ballarotto, K. Siegrist, R.J. Phaneuf, E.D. Williams, S. Mogren, Surface Science **461** (2000) L570-L574.

[10] V.W. Ballarotto, K. Siegrist, R.J. Phaneuf, E.D. Williams, W.C. Yang, R.J. Nemanich, Applied Physics Letters **78** (2001) 3547-3549.

[11] V.W. Ballarotto, M. Breban, K. Siegrist, R.J. Phaneuf, E.D. Williams, Journal of Vacuum Science & Technology B **20** (2002) 2514-2518.

[12] K. Siegrist, V.W. Ballarotto, M. Breban, R. Yongsunthon, E.D. Williams, Applied Physics Letters **84** (2004) 1419-1421.

[13] K. Siegrist, V.W. Ballarotto, E.D. Williams, Advanced Data Storage Materials and Characterization Techniques **803** (2004) 9-14
280.

[14] L. Frank, I. Mullerova, D.A. Valdaitsev, A. Gloskovskii, S.A. Nepijko, H.J. Elmers, G. Schonhense, Journal of Applied Physics **100** (2006) XX-XX.

[15] M. Mankos, D. Adler, L. Veneklasen, E. Munro, Surface Science **601** (2007) 4733-4741.

[16] M.L. Anderson, C.Y. Nakakura, K.F. Saiz, G.L. Kellogg, in: E. Snoeck, R. Dunin-Borkowski, J. Verbeeck, U. Dahmen (Eds.), Quantitative Electron Microscopy for Materials Science, Warrendale, PA, 2008, pp. 1026-C15-03.

[17] E. Bauer, Reports on Progress in Physics **57** (1994) 895-938.

DISTRIBUTION

1	MS0123	D. Chavez, LDRD Office	1011
2	MS0899	Technical Library	9536 (electronic copy)
1	MS062	M. L. Anderson	5644
2	MS9018	Central Technical Files	8944

Sandia National Laboratories